Circular Filters for Target Tracking in 3D

Dirk Tenne
Mechanical & Aerospace Engineering
University at Buffalo
Buffalo, NY 14260
USA
tenne@eng.buffalo.edu

Tarunraj Singh
Mechanical & Aerospace Engineering
University at Buffalo
Buffalo, NY 14260
USA
tsingh@eng.buffalo.edu

Abstract – *This paper describes the development of a three dimensional geometrically constrained target tracker. This tracker combines the predictions of a circular prediction algorithm and a constant velocity filter by utilizing the Covariance Intersection. This combined prediction can be updated with the consequent measurement using the linear estimator. The proposed technique is illustrated on a benchmark trajectory including circular and straight line maneuvers.*

Keywords: Circular filter, tracking, three dimensions, hybrid filter.

1 Introduction

The estimation and prediction of the kinematics of a dynamic object requires the use of a dynamic model and discrete time data. A majority of target trackers are based on a straight line maneuver, where model uncertainties and man-made disturbances are accounted for as stochastic acceleration. In contrast to the simple straight line filters, complex non-linear models have been developed to capture the real object dynamics which are applied to special maneuvers such as the coordinated turns. The focus of this paper is on the development of a non-model based algorithm which constrains the predicted state to a circular turn.

1.1 Coordinated Turn Models

Filters based on a constant velocity or constant acceleration trajectory are implemented as α-β [1, 2, 3], α-β-γ [4, 5] and linear Kalman filters [6, 7, 8]. Singer [9] developed an acceleration model for manned maneuvering targets with exponentially autocorrelated acceleration. He viewed this acceleration as perturbations upon the constant velocity trajectory. Relaxing the straight line assumption, Berg [10] augmented Singer's model by an "adaptive estimation of the mean target jerk", which is the result of a coordinated turn. The coordinated turn is a special maneuver, which is consistent with the bank-to-turn flight characteristics of a fixed-wing aircraft [11]. This planar maneuver is defined by assuming (i) the aerodynamic lift (L) and the resulting thrust (T) are constant and (ii) the roll rate (p) is zero. This algorithm is based on aircraft related parameters like thrust, lift and target inertial angular velocity components (p, q, r), which form a set of coupled non-linear differential equations. Bishop and Antoulas [12, 13] treated the aircraft as a material point as a result of assuming the angle of attack (α_x) and sideslip (β) to be zero. In combination with the coordinated turn assumptions, this algorithm reduces to a kinematics problem. In contrast to Berg's augmented adaptive jerk model, the prediction equation becomes non-linear, but does not require the explicit calculation of L, T, p, q, r. This algorithm can be simplified by assuming constant speed during the coordinated turn, which leads to a constant turn rate vector Ω [14, 15]. Nabaa and Bishop [16] have shown that the constant speed coordinated turn is a particular subset of the general coordinated turn of Bishop and Antoulas. In general the coordinated turn models are a set of non-linear, coupled equations, which are difficult to solve.

1.2 Geometrically Constraining Methods

A geometric approach of implementing a circular turn has been developed by Roecker and McGillem [17], and a similiar approach by Kawase et al. [18]. The circular prediction is constrained to lie on a circle, whose center is estimated based on previous measurements. The center-point-approach (CPA) predicts in a polar coordinate system (R and ψ) whose origin is the center of the circle. The CPA is not amenable for further stability, performance and uncertainty analysis, because of the complex center coordinate calculation and discontinuities in the polar angle ψ between successive scans. This discontinuity appears by switching from the previous circle to the next circle as the radius and center change. Tenne and Singh [19] proposed a circular prediction algorithm, which integrates the measured data into the filter and constrains the prediction to lie on the arc of a circle. The circular prediction algorithm is defined in relative coordinates without the requirement of calculating the center and the radius.

2 Circular Motion Target Model in 2D

To develop the algorithm, consider four points lying on a circle as shown in Fig. 1(a). The four points are connected to create two triangles $\triangle 123$ and $\triangle 134$, where the triangle sides are named by the points which they

connect, for example, R_{12} is the distance between points ① and ②. The fourth point can be described relative to the points ① to ③ by a variety of angle and distance combinations. A convenient pair is the angle φ_2 and the distance R_{34} as indicated in Fig. 1. The desired

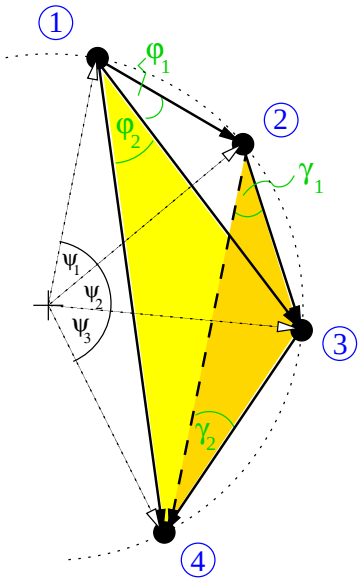

(a) Basic Properties

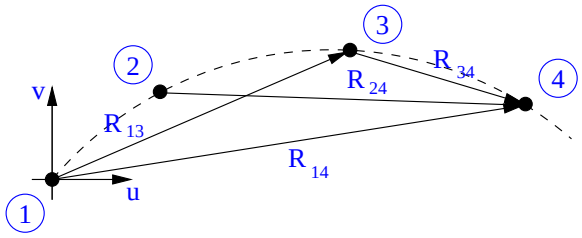

(b) Relative Relationships

Fig. 1: Properties of points lying on a circle

prediction equations define the relationships between the fourth point, which is parameterized by R_{34} and φ_2 and the previous three points. To derive the prediction equation, consider the points ②, ③ and ④ relative to point ①, which is equivalent to introducing a Cartesian coordinate system labeled u-v with its origin at point ①. Observing Fig. 1(b), the distances are defined in terms of u_i and v_i.

$$R_{13}^2 = u_3^2 + v_3^2 \quad (1a)$$
$$R_{14}^2 = u_4^2 + v_4^2 \quad (1b)$$
$$R_{24}^2 = (u_4 - u_2)^2 + (v_4 - v_2)^2 \quad (1c)$$
$$R_{34}^2 = (u_4 - u_3)^2 + (v_4 - v_3)^2 \quad (1d)$$

(1c) and (1d) can be rewritten as:

$$u_2u_4 + v_2v_4 = R_{12}R_{14}\cos(\varphi_1 + \varphi_2) \quad (2a)$$
$$u_3u_4 + v_3v_4 = R_{13}R_{14}\cos(\varphi_2)\ , \quad (2b)$$

and solving for the relative position $[u_4\ v_4]^T$, yields the desired relationship

$$\begin{bmatrix} u_4 \\ v_4 \end{bmatrix} = \begin{bmatrix} u_2 & v_2 \\ u_3 & v_3 \end{bmatrix}^{-1} \begin{bmatrix} R_{12}\cos(\varphi_1 + \varphi_2) \\ R_{13}\cos(\varphi_2) \end{bmatrix} R_{14}\ . \quad (3)$$

The unknown distance R_{14} in (3) is determined from $\triangle 134$ using the cosine rule

$$R_{14} = R_{13}\left[\cos(\varphi_2) + \sqrt{\left(\frac{R_{34}}{R_{13}}\right)^2 - \sin^2(\varphi_2)}\right]\ , \quad (4)$$

The solution of R_{14} contains the evaluation of a square root, whose radicand can take negative values. It is therefore, desirable to derive an alternative form, which proves advantageous in the prospective development. By replacing $R_{34} = \sin\varphi_2/\sin\varphi_1 R_{23}$ the equation for R_{14} can be rewritten as:

$$R_{14} = R_{13}\cos(\varphi_2) + \frac{\sin(\varphi_2)}{\sin(\varphi_1)}\sqrt{R_{23}^2 - R_{13}^2\sin^2(\varphi_2)} \quad (5)$$

The square root expression can be modified by observing Figure 2, where the triangle $\triangle 123$ has been extended in the direction of the phasor R_{12}, to build a right angle triangle with the hypotenuse R_{13}.

$$\sqrt{R_{23}^2 - R_{13}^2\sin^2(\varphi_2)} = R_{13}\cos(\varphi_1) - R_{12}$$

Further simplification with the use of the sum of angle

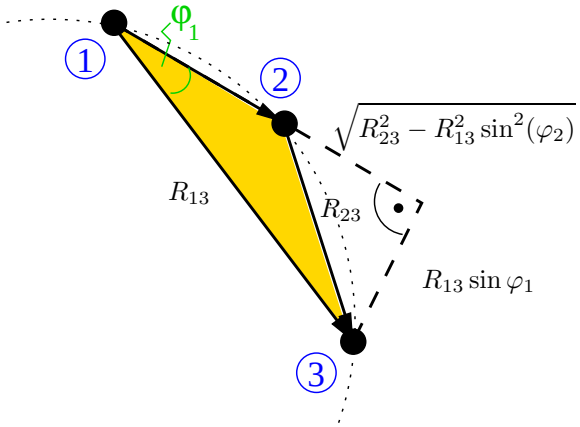

Fig. 2: Right angle triangle extension to triangle $\triangle 123$

theorem leads to

$$R_{14} = \left[R_{13}\sin(\varphi_1 + \varphi_2) - R_{12}\sin(\varphi_2)\right]\frac{1}{\sin(\varphi_1)}\ . \quad (6)$$

Note that equation 6 is also valid for straight line maneuvers. Assuming that the prediction angle φ_2 can be expressed in terms of φ_1 as $\varphi_2 = k\varphi_1$ and noticing that φ_1 equals zero for a straight line, equation 6 reduces to

$$\lim_{\varphi_1 \to 0} R_{14} = R_{13} + k(R_{13} - R_{12}), \quad (7)$$

where the l'Hospital rule has been applied. The difference $R_{13} - R_{12}$ equals the distance R_{23} and the predicted distance is the sum of R_{13} and a scaled R_{23}. Assuming a constant speed (cs) angular turn, equation 6 reduces to

$$R_{14}^{\mathrm{cs}} = 2R_{13}\cos(\varphi_2) - R_{12} \ , \tag{8}$$

and in the case of a straight line maneuver

$$\lim_{\varphi_1 \to 0} R_{14}^{\mathrm{cs}} = 2R_{13} - R_{12} \ . \tag{9}$$

For prospective development of a 3 dimensional extension of the planar algorithm, the prediction equation in relative Cartesian coordinates can be interpreted as a vector quantity. Define the vector $\vec{r}_{12}$ of length R_{12} pointing from point ① towards point ②, and vector $\vec{r}_{13}$ respectively. By evaluating the matrix inverse

$$\begin{bmatrix} u_2 & v_2 \\ u_3 & v_3 \end{bmatrix}^{-1} = \frac{1}{u_2 v_3 - u_3 v_2} \begin{bmatrix} v_3 & -v_2 \\ -u_3 & u_2 \end{bmatrix} \tag{10}$$

and noticing that the determinant can be expressed as:

$$u_2 v_3 - u_3 v_2 = R_{12} R_{13} \sin\varphi_1 \ , \tag{11}$$

which is a direct result of the cross product performed in a 2 dimensional plane

$$\|\vec{r}_{13} \times \vec{r}_{12}\| = \|\vec{r}_{13}\| \|\vec{r}_{12}\| \sin(\varphi_1) = R_{12} R_{13} \sin(\varphi_1) \tag{12}$$

the prediction equation can be rewritten as:

$$\begin{bmatrix} u_4 \\ v_4 \end{bmatrix} = T(\pi/2)\vec{n}_{13} R_{14} \frac{\cos(\varphi_1 + \varphi_2)}{\sin(\varphi_1)} + T(-\pi/2)\vec{n}_{12} R_{14} \frac{\cos(\varphi_2}{\sin(\varphi_1} \tag{13}$$

The following substitutions have been introduced. The matrix $T(\alpha)$ is the rotational transformation matrix defined as

$$T(\alpha) = \begin{bmatrix} \cos(\alpha) & \sin(\alpha) \\ -\sin(\alpha) & \cos(\alpha) \end{bmatrix} \ . \tag{14}$$

The normalized vector $\vec{n}_{12}$ is the unit vector pointing in the direction of $\vec{r}_{12}$. The new prediction equation 13 consists of a summation of the rotated and scaled unit vectors $\vec{n}_{12}$ and $\vec{n}_{13}$ in a 2 dimensional plane. In a three dimensional environment the same rotation has to be performed around the normal vector defined by the two dimensional plane.

3 3D Circular Motion Estimation

Real world targets operate in three space and consequently trackers cannot be constrained to predict in two dimensions. The radar measurements, for example, are obtained in a spherical coordinate system reporting the range, azimuth and elevation, whereas the target's position is described in a global Cartesian coordinate system. The proposed curve-fitting estimator constrains the prediction to a circular trajectory in a two dimensional coordinate system. This section addresses the fact that the three points form a two dimensional plane, which is oriented in three dimensions. The circular estimation can be performed in this two dimensional plane and later back-transformed to the global three dimensional coordinate system.

3.1 Representing the Circular Prediction Plane

The circular prediction algorithm described in section 2 is performed based on three position measurements. These three locations define two vectors $\vec{r}_{12}$ and $\vec{r}_{13}$, which span a two dimensional plane in a three dimensional space. For illustrative purposes let us assume three points in space be (i) at the origin, (ii) on the x-z plane at $[1\ 0\ 1]$, and (iii) on the y-z plane at $[0\ 1\ 1]$. The normal vector $\vec{n}_s$ of the 2D plane can be obtained by evaluating the cross product.

$$\vec{n}_s = \frac{\vec{r}_{12} \times \vec{r}_{13}}{\|\vec{r}_{12} \times \vec{r}_{13}\|} \tag{15}$$

The orientation of the normal vector is positive when the three vectors constitute a right-handed coordinate system, which can also be determined by the right-hand screw rule rotating $\vec{r}_{12}$ into the direction of $\vec{r}_{13}$. Figure 3 displays the three points marked by the symbol '×' and the normal vector denoted by the symbol '□'. It also illustrates the x-y plane of the global Cartesian coordinate system. The transition from the original Cartesian

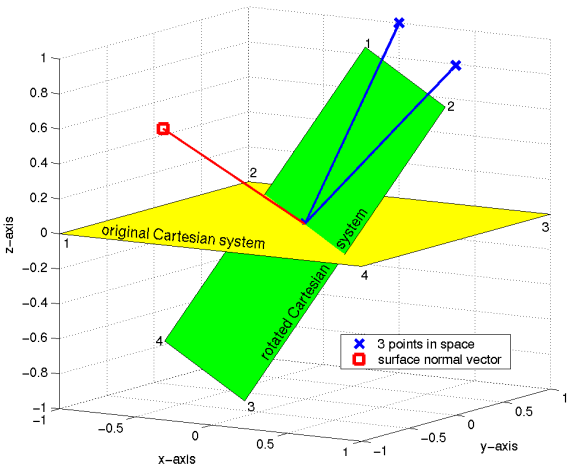

Fig. 3: Circular Prediction Plane

coordinate system to the circular prediction plane can be achieved by a multi-step rotation of the coordinate system. The first step consists of a rotation around the z-axis such that the projection of the normal vector on to the x-y plane aligns with the x-axis. This rotation is performed by the three dimensional transformation matrix

$$G_1 = \begin{bmatrix} \cos(\varphi_s) & \sin(\varphi_s) & 0 \\ -\sin(\varphi_s) & \cos(\varphi_s) & 0 \\ 0 & 0 & 1 \end{bmatrix} \ , \tag{16}$$

where φ_s is the polar rotation angle of the normal vector projected on to the x-y plane. Subsequent to the alignment of the x-axis, the second step rotates the coordinate system around the transformed y-axis. This rotation is performed by the rotation matrix

$$G_2 = \begin{bmatrix} \cos(\vartheta_s) & 0 & -\sin(\vartheta_s) \\ 0 & 1 & 0 \\ \sin(\vartheta_s) & 0 & \cos(\vartheta_s) \end{bmatrix} \ , \tag{17}$$

where ϑ_s is the direction cosine of the normal vector with respect to the z-axis. The combined coordinate transformation can be obtained by constructing the rotation matrix consisting of G_1 and G_2:

$$G = G_2 G_1 \tag{18}$$

Note that the rotation matrices G_i are orthogonal and thus $G_i^{-1} = G_i^T$.

3.2 Extended Circular Prediction Algorithm to Three Dimensions

Based on the development of the two dimensional circular prediction algorithm (Section 2) and the results of the circular prediction plane, this section describes the circular prediction algorithm in three dimensional space. Conceptually, the circular prediction is performed on a two dimensional plane, which is defined by the three circular points, i.e. the vectors $\vec{r}_{12}$ and $\vec{r}_{13}$ span the circular prediction plane. The fact, that the circular prediction can be described as a rotation of these two vectors can be exploited to extend the algorithm to include the third dimension. Equation 13 can be rewritten to include a zero z-component of the predicted position and the normalized vectors, where the rotation matrix $T(\alpha)$ can be defined as:

$$T(\alpha) = \begin{bmatrix} \cos(\alpha) & \sin(\alpha) & 0 \\ -\sin(\alpha) & \cos(\alpha) & 0 \\ 0 & 0 & 1 \end{bmatrix} . \tag{19}$$

Substituting the normalized vectors with vectors described in the relative Cartesian coordinates, equation 13 can be written as:

$$\begin{bmatrix} u_4 \\ v_4 \\ 0 \end{bmatrix} = T(\pi/2) G \begin{bmatrix} u_3' \\ v_3' \\ w_3' \end{bmatrix} \frac{R_{14}}{R_{13}} \frac{\cos(\varphi_1 + \varphi_2)}{\sin(\varphi_1)} + T(-\pi/2) G \begin{bmatrix} u_2' \\ v_2' \\ w_2' \end{bmatrix} \frac{R_{14}}{R_{12}} \frac{\cos(\varphi_2)}{\sin(\varphi_1)} , \tag{20}$$

where G is given by equation 18. The circular prediction of equation 20 is described with respect to a Cartesian coordinates system where the x-y plane coincides with the circular prediction plane. Including the back transformation into equation 20

$$\begin{bmatrix} u_4' \\ v_4' \\ w_4' \end{bmatrix} = G^{-1} \begin{bmatrix} u_4 \\ v_4 \\ 0 \end{bmatrix} \tag{21}$$

involves the evaluation of the matrix product

$$\mathcal{G} = G^{-1} T(\pi/2) G \tag{22}$$

Note, since $T(-\pi/2) = T^T(\pi/2)$ and G is orthogonal it can be shown that the combined transformation matrix $G^{-1} T(-\pi/2) G = \mathcal{G}^T$. Therefore, the circular prediction performed on the 2D plane can be written with respect to the global Cartesian coordinate system as:

$$\begin{bmatrix} u_4' \\ v_4' \\ w_4' \end{bmatrix} = \mathcal{G} \begin{bmatrix} u_3' \\ v_3' \\ w_3' \end{bmatrix} \frac{R_{14}}{R_{13}} \frac{\cos(\varphi_1 + \varphi_2)}{\sin(\varphi_1)} + \mathcal{G}^T \begin{bmatrix} u_2' \\ v_2' \\ w_2' \end{bmatrix} \frac{R_{14}}{R_{12}} \frac{\cos(\varphi_2)}{\sin(\varphi_1)} \tag{23}$$

By adding the coordinates of the first point and substituting the relative coordinates with the global coordinates, we obtain the circular prediction in global Cartesian coordinates.

$$\begin{bmatrix} x_4 \\ y_4 \\ z_4 \end{bmatrix} = \mathcal{G} \begin{bmatrix} x_3 \\ y_3 \\ z_3 \end{bmatrix} s_1 + \mathcal{G}^T \begin{bmatrix} x_2 \\ y_2 \\ z_2 \end{bmatrix} s_2 + (I - \mathcal{G} s_1 - \mathcal{G}^T s_2) \begin{bmatrix} x_1 \\ y_1 \\ z_1 \end{bmatrix} \tag{24}$$

where the abbreviations:

$$s_1 = \frac{R_{14}}{R_{13}} \frac{\cos(\varphi_1 + \varphi_2)}{\sin(\varphi_1)} \tag{25}$$

$$s_2 = \frac{R_{14}}{R_{12}} \frac{\cos(\varphi_2)}{\sin(\varphi_1)} \tag{26}$$

have been introduced.

Figure 4 illustrates the circular prediction in a three dimensional space. It shows the x-y plane of the global Cartesian coordinate system and the projection of the three points in a 3D space as well as their connecting circle. Performing the circular prediction with equation 24, we obtain a position on the circular prediction plane which is furthermore constrained to lie on a circle defined by the three measurements.

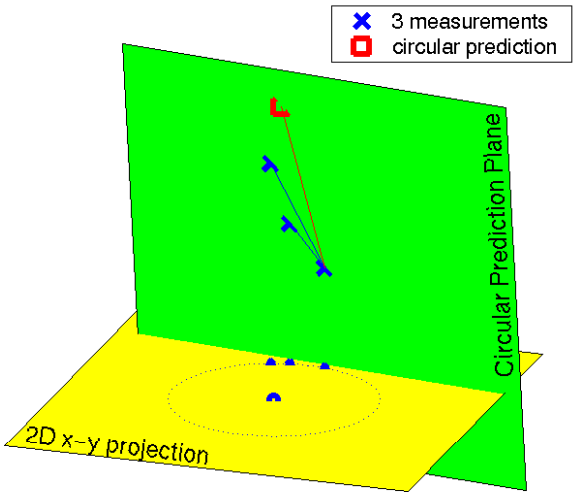

Fig. 4: Circular Prediction in a 3D space.

3.3 Extended Curve-fitting Approach and Hybrid Filters

The prediction algorithms constraining the target motion on a smooth curve provide a reasonable performance for circle like trajectories. However, real target motions can be approximated by piecewise curves which are circles and straight lines. In addition with the presence of noise,

the performance of a stand-alone circular filter would degrade. The proposed circular filter is therefore integrated with traditional filters including straight line target models.

A common model used, assumes a target moving on a straight line with a constant velocity, where the system is driven by white noise acceleration. The linear state space is comprised of the x,y,z position as well as the three velocities v_x, v_y and v_z. The radar measurements are obtained in the spherical coordinate system reporting the range (R), azimuth (ψ) and elevation (ϑ), which are related to the Cartesian coordinate system centered at the radar location. The conversion can be derived as:

$$R = \sqrt{x^2+y^2+z^2} \quad (27)$$

$$\psi = \arctan\frac{y}{x} \quad (28)$$

$$\vartheta = \arctan\frac{\sqrt{x^2+y^2}}{z} = \arccos\frac{z}{R} \quad (29)$$

Employing the extended Kalman filter the Jacobian of the output equation is required, which can be derived as:

$$H = \begin{bmatrix} \frac{x}{R} & \frac{y}{R} & \frac{z}{R} & 0 & 0 & 0 \\ \frac{-y}{\check{R}^2} & \frac{x}{\check{R}^2} & 0 & 0 & 0 & 0 \\ \frac{xz}{R^2\check{R}} & \frac{yz}{R^2\check{R}} & -\frac{\check{R}}{R^2} & 0 & 0 & 0 \end{bmatrix} , \quad (30)$$

where $\check{R}^2 = x^2+y^2$. Subsequently, the extended Kalman filter equations have to be applied. This model is driven by white noise acceleration, which can be best described in the target's coordinate frame, where the Cartesian abscissa is aligned with the heading direction. The accelerations as shown in Figure 5 are divided into the parallel acceleration a_p, the normal acceleration a_n, and the binormal acceleration a_b, where the variances are σ_p^2, σ_n^2 and σ_b^2 respectively. The process noise covariance can be

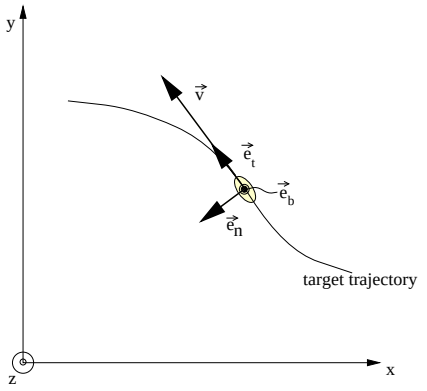

Fig. 5: Target Accelerations in the natural coordinate system

calculated by a discretized white noise model and using the inverse 3D rotation matrix of equation 18. With the aforementioned derivation, it is relatively easy to program the extended Kalman filter algorithm.

The unscented transformation is utilized to perform the circular prediction, which is fused via Covariance Intersection with the linear prediction. The circular prediction on the 3D prediction plane is described by equation 24, which depends on the three position measurements. These are generally obtained by a radar in spherical coordinates. To obtain the statistics of the circular prediction, the three measurements are stacked to form an augmented vector

$$\mathbf{x} = \begin{bmatrix} r_1 & \psi_{r1} & \vartheta_{r1} & r_2 & \psi_{r2} & \vartheta_{r2} & r_3 & \psi_{r3} & \vartheta_{r3} \end{bmatrix}^T \quad (31)$$

consisting of the radar reports as range r, azimuth ψ_r and elevation ϑ_r. Its covariance is a diagonal matrix with the repeated elements of the individual covariances σ_r^2, σ_ψ^2 and σ_ϑ^2. The unscented transformation can be applied to the augmented space, where the σ points are transformed to a Cartesian coordinate system and further propagated with the circular prediction equation. Figure 6 illustrates the σ-set and the propagation on an example configuration. The position uncertainties are symbolized by the 1-σ covariance ellipsoids.

The standard unscented transformation creates 19 circular trajectories i.e. 19 possible combinations of the three uncertain measurements, to determine the statistics of the circular prediction. The small squares '□' indicate these predictions, which result in the mean and covariance by evaluating the weighted sum. The mean and covariance are illustrated by the large square '□' and the prediction ellipsoid.

The hybrid filter consists of a convex combination of the circular prediction and the predicted position of the extended Kalman filter. These predictions are statistically correlated since they are conditioned on the same measurements. Therefore, the fusion is performed using the Covariance Intersection (CI) algorithm developed by Uhlmann [20]. In contrast to the Kalman filter update, the CI does not assume independent data to be fused, thus yielding a conservative fusing algorithm. Assume two random processes A and B, which are described by their mean (a, b) and covariance (P_a, P_b). Uhlmann has arrived at the CI algorithm by showing that the solution of a conservative fusion yielding a positive definite error covariance is a function of a scalar weight w only. He used the matrix contraction theorem to arrive at the two fusion equations:

$$P_c^{-1} = wP_a^{-1} + (1-w)P_b^{-1} , \quad (32)$$

$$P_c^{-1}\mathbf{c} = wP_a^{-1}\mathbf{a} + (1-w)P_b^{-1}\mathbf{b} \quad (33)$$

where w takes values in the range of $[0,1]$. The weight w can be interpreted as a tuning parameter of the CI. Its selection shapes the estimated covariance either closer to the covariance of A ($w \to 1$) or to the covariance of B ($w \to 0$). This combined prediction can be updated with the consequent measurement using the linear estimator.

4 Benchmark Trajectory

This section presents the performance characteristics of the proposed hybrid filter compared to the straight line constant velocity filter. The benchmark trajectory includes a combination of coordinated turns and straight line maneuvers. Figure 7 illustrates the target maneuver consisting of three parts in the x-y plane:

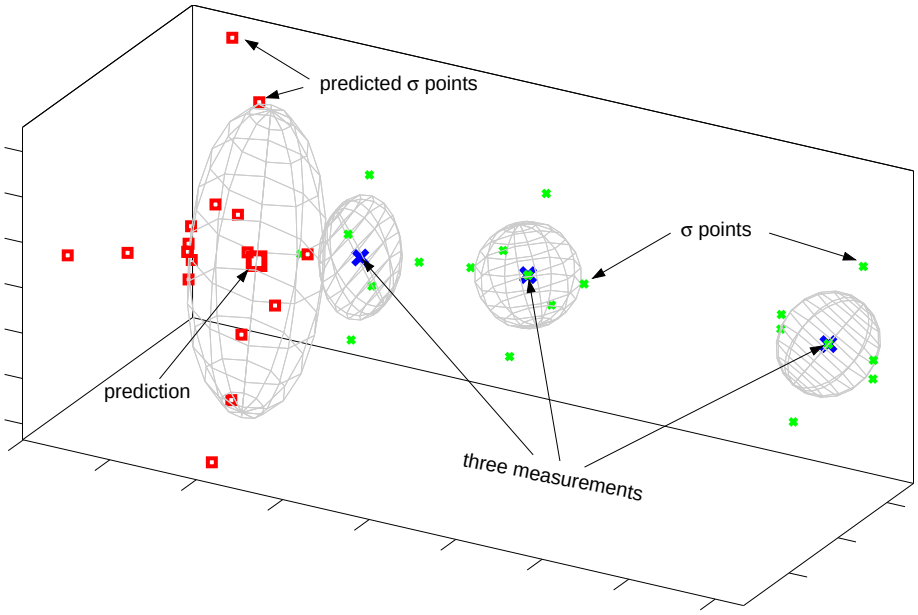

Fig. 6: Unscented σ-set illustrated on the circular prediction

- a circular trajectory with constant angular velocity
- a straight line maneuver with constant speed
- an accelerating target on a circular trajectory.

The targets elevation is simulated as an up-and-down maneuver comparable to a sine function. The targets position is reported by a radar located at the circled position as range-bearing measurements. A sample of measurements is indicated by the markers $\times$.

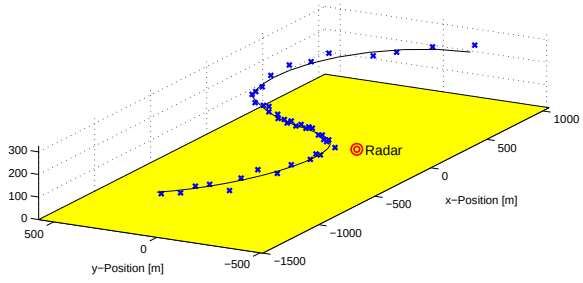

Fig. 7: Benchmark Target Maneuver with Sample Measurements

To test the hybrid filter's optimality, a consistency test as described in [21] has been carried out. The hypothesis H_0 postulates that the normalized estimation error squared (NEES) equals the dimension of the state. Performing a Monte Carlo simulation the hypothesis H_0 can be accepted if the test statistic lies in the two-sided 95% probability concentration region. Figure 8 shows this region along with the average NEES based on 100 Monte Carlo runs. Only a small part lies outside the 95% region and the H_0 hypothesis can be accepted.

A statistical comparison of the filters can be achieved by a simple hypothesis test. Define the performance measure as the root-mean-square error of the filter's estimation error:

$$\epsilon_{\text{filter}}(k) = E\{e_{\text{filter}}(k|k)\} \tag{34}$$

where $e_{\text{filter}}(k|k)$ is the estimation error compared to the true target position. Let us postulate the hypothesis that the error of filter 1 is larger than the error of filter 2:

$$H_1: \quad \Delta(k) = \epsilon_{\text{filter1}}(k) - \epsilon_{\text{filter2}}(k) > 0 \tag{35}$$

Based on Monte Carlo simulations the test statistic

$$\mu(k) = \frac{\bar{\Delta}(k)}{\sigma_\Delta(k)} \tag{36}$$

can be calculated, where the $\bar{\Delta}$ corresponds to the mean of $\Delta(k)$ and $\sigma_\Delta(k)$ represents the deviation. If μ exceeds a threshold μ_0 than the hypothesis H_1 is accepted. The threshold is commonly defined by the significance level of the null hypothesis.

The statistical test is performed to compare the performance of the straight line (sl) model to the combined straight line and circular prediction (hybrid) model. The hypothesis is postulated as

$$H_1: \quad \Delta(k) = \epsilon_{\text{sl}}(k) - \epsilon_{\text{hybrid}}(k) > 0\ . \tag{37}$$

The second hypothesis (H_2) compares the circular filter with the hybrid filter. Both test statistics are shown in

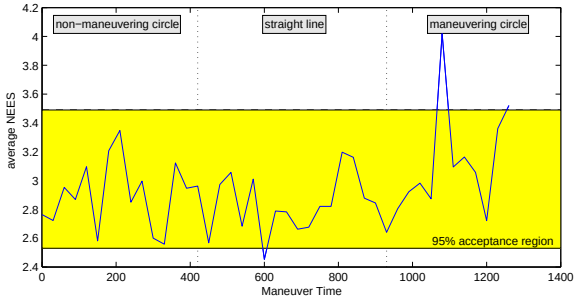

Fig. 8: Consistency Test of the Hybrid 3D filter

Figure 9. The hypothesis H_1 compares the hybrid filter with the EKF using a straight line model, and it can be observed that the hybrid filter performs better during the circular maneuver since the test statistic is above the threshold, whereas during the straight line maneuver the test statistic falls below the threshold. The comparison of the circular filter and the hybrid filter yields better performance for the circular filter during the turning maneuvers and the hybrid filter exhibits improved performance during the straight line maneuver.

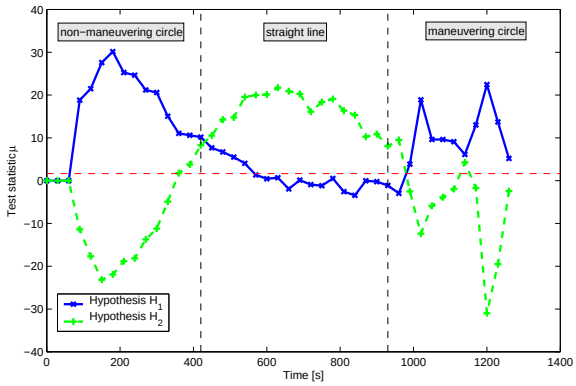

Fig. 9: Statistical Test Comparison of Hypotheses H_1 and H_2

5 Conclusions

A simple technique to predict 3D motion of targets assuming that they lie on an arc of a circle had been developed. Using this filter in conjunction with a set of straight line filters, has resulted in improved performance compared to classic extended Kalman filters. The unscented transformation has been exploited to determine the covariance of the estimates of the circular filter and the circular filter estimate has been fused with the straight line filter using the Covariance Intersection algorithm.

The proposed filter in 2D or 3D can compliment the bank of filters in an Interactive Multiple Model (IMM) filter or the Variable Dimension (VD) filter. Maneuver detectors can also be exploited to switch between different target models describing various maneuvers of the target.

References

[1] Jack Sklansky. Optimizing the dynamic parameter of a track-while-scan system. *RCA Laboratories, Princton, NJ*, June 1957.

[2] T. R. Benedict and G. W. Bordner. Synthesis of an optimal set of radar track-while-scan smoothing equations. In *IRE Transactions on Automatic Control*, volume AC-1, July 1962.

[3] Paul R. Kalata. $\alpha-\beta$ target tracking systems: A survey. In *ACC*, 1992.

[4] H. R. Simpson. Performance measures and optimization condition for a third order sampled-data tracker. In *IEEE Trans. on Automat. Contr.*, volume AC-12, June 1962.

[5] Paul R. Kalata. The tracking index: A generalized parameter for $\alpha-\beta$ and $\alpha-\beta-\gamma$ target trackers. In *IEEE Trans. Aerosp. and Electron. Syst.*, volume AES-20, No.2, Mar. 1984.

[6] Yaakov Bar-Shalom and Thomas E. Fortmann. *Tracking and Data Association*. Academic Press, Inc., 1988.

[7] John A. Lawton, Robert J. Jesionowski, and Paul Zarchan. Comparison of four filtering options for radar tracking problem. *J. of Guid., Cont. and Dyn.*, 21(4), July 1998.

[8] A.T. Alouani, P. Xia, T.R. Rice, and W.D. Blair. A two-stage kalman estimator for tracking maneuvering targets. In *IEEE Int. Conf. on Sys., Man., and Cybernetics*, volume 2, 1991.

[9] R. A. Singer. Estimating optimal tracking filter performance for manned maneuvering targets. In *IEEE Trans. Aerosp. and Electron. Syst.*, volume AES-5, Nov. 1970.

[10] Russell F. Berg. Estimation and prediction for maneuvering target trajectories. In *IEEE Trans. on Automat. Contr.*, volume AC-28, pages 294–304, Mar. 1983.

[11] R. von Mises. *Theory of Flight*. McGraw-Hill Book Co., New York, 1945.

[12] R. H. Bishop and A. C. Antoulas. Non-linear approach to the aircraft tracking problem. In *Proc. of the AIAA Guidance, Navigation and Control Conference*, volume 1, pages 692–703, New Orleans, LA, Aug. 1991.

[13] R. Bishop and A. C. Antoulas. Non-linear approach to the aircraft tracking problem. *J. of Guid., Cont. and Dyn.*, 17(5):1124–1130, Sept. 1994.

[14] S. Blackman and R. Popoli. *Design Analysis of Modern Tracking Systems*. Artech House, Norwood, MA, 1999.

[15] T.E. Bullock and S. Sangsuk-Iam. Maneuver detection and tracking with a nonlinear target model. In *Proc. of the Conf. on Decision and Control*, volume 1, pages 1122–1126, Las Vegas, NV, Dec. 1984.

[16] N. Nabaa and R. H. Bishop. Validation and comparison of coordinated turn aircraft maneuver models. In *IEEE Trans. Aerosp. and Electron. Syst.*, volume 36, pages 250–259, Jan. 2000.

[17] James A. Roecker and Clare D. McGillem. Target tracking in maneuver-centered coordinates. *IEEE Trans. Aerosp. and Electron. Syst.*, 25(6):836–843, Nov. 1989.

[18] T. Kawase, H. Tsarunosono, N. Ehara, and I. Sasase. An adaptive-gain alpha-beta tracker combined with circular prediction for maneuvering target tracking. In *IEEE TENCON*, volume 2, 1997.

[19] Dirk Tenne and Tarunraj Singh. Circular prediction algorithms – hybrid filters. In *ACC*, May 2002.

[20] Jeffrey Uhlmann, Simon Julier, Behzad Kamgar-Parsi, Marco Lanzagorta, and Haw-Jye Shyu. NASA Mars Rover: A testbed for evaluating applications of covariance intersection. In *Proc. of the 1999 Unmanned Ground Vehicle Technology*, volume 3693, pages 140–149, Washington, DC, USA, 1999. Naval Research Lab, Proc. of SPIE - The Int. Society for Optical Eng.

[21] Yaakov Bar-Shalom and Xiao-Rong Li. *Estimation and Tracking: Principles, Techniques and Software*. YBS, 1998.